J. Cell. Mol. Med. Vol 12, No 2, 2008 pp. 479-495

Acetylcholinesterase-R increases germ cell apoptosis but enhances sperm motility

I. Mor [a], E. H. Sklan [a], E. Podoly [a], M. Pick [a, b], M. Kirschner [a], L. Yogev [c], S. Bar-Sheshet Itach [d], L. Schreiber [e], B. Geyer [f], T. Mor [f], D. Grisaru [g], H. Soreq [a, *]

[a] The Silberman Institute of Life Sciences, the Hebrew University of Jerusalem, Jerusalem, Israel
[b] Institute of Hematology, Tel Aviv Sourasky Medical Center, Sackler Faculty of Medicine, Tel-Aviv University, Israel
[c] Institute for the Study of Fertility, Tel Aviv Sourasky Medical Center, Sackler Faculty of Medicine, Tel-Aviv University, Israel
[d] The Mina&Everard Faculty of Life Sciences, Bar-Ilan University, Ramat-Gan, Israel
[e] Institute of Pathology, Tel Aviv Sourasky Medical Center, Sackler Faculty of Medicine, Tel-Aviv University, Israel
[f] Arizona Biodesign Institute, Arizona State University, Tempe, AZ, USA
[g] Department of Obstetrics and Gynecology, Tel Aviv Sourasky Medical Center, Sackler Faculty of Medicine, Tel-Aviv University, Israel

Received: September 28, 2007; Accepted: January 4, 2007

Abstract

Changes in protein subdomains through alternative splicing often modify protein-protein interactions, altering biological processes. A relevant example is that of the stress-induced up-regulation of the acetylcholinesterase (AChE-R) splice variant, a common response in various tissues. In germ cells of male transgenic TgR mice, AChE-R excess associates with reduced sperm differentiation and sperm counts. To explore the mechanism(s) by which AChE-R up-regulation affects spermatogenesis, we identified AChE-R's protein partners through a yeast two-hybrid screen. In meiotic spermatocytes from TgR mice, we detected AChE-R interaction with the scaffold protein RACK1 and elevated apoptosis. This correlated with reduced scavenging by RACK1 of the pro-apoptotic TAp73, an outcome compatible with the increased apoptosis. In contrast, at later stages in sperm development, AChE-R's interaction with the glycolytic enzyme enolase-α elevates enolase activity. In transfected cells, enforced AChE-R excess increased glucose uptake and adenosine tri-phosphate (ATP) levels. Correspondingly, TgR sperm cells display elevated ATP levels, mitochondrial hyperactivity and increased motility. In human donors' sperm, we found direct association of sperm motility with AChE-R expression. Interchanging interactions with RACK1 and enolase-α may hence enable AChE-R to affect both sperm differentiation and function by participating in independent cellular pathways.

Keywords: acetylcholinesterase • protein-protein interaction • spermatogenesis • apoptosis • glycolysis

Introduction

Protein–protein interactions are a key factor in determining proteins' biochemical and signalling characteristics, subcellular localization, and stability. Therefore, deciphering networks of protein interactions, the 'interactome', is crucial to our understanding of biological processes [1]. Combinatorial modulation of the cellular proteome enriches the biological processes that can be executed, especially during differentiation, which requires dynamic, meticulously orchestrated specialization events. Spermatogenesis provides an exquisite

*Correspondence to: Hermona SOREQ,
The Silberman Inst. of Life Sciences, The Hebrew University of Jerusalem, Safra Campus- Givat Ram, Jerusalem 91904, Israel.
Tel.: +972-26585109; Fax: +972-26586448
E-mail: soreq@cc.huji.ac.il

doi: 10.1111/j.1582-4934.2008.00231.x

example of continuous terminal differentiation, whereby spermatogonia stem cells divide continuously to form meiotic spermatocytes, which yield haploid spermatids that are ultimately transformed into spermatozoa.

The acetylcholine hydrolyzing enzyme acetylcholinesterase (AChE) is classically known for terminating cholinergic neurotransmission. However, sperm cells from many animal species, human beings and rodents included, display AChE activity [2] localized to sperm tails [3]. Several AChE variants are known, which share a common core domain, but differ in their C-terminus as a result of alternative splicing. This primarily contributes to the non-enzymatic roles of AChE [4]. For example, through its unique C-terminal region, the stress-induced AChE-R variant binds RACK1 (receptor of activated protein kinase C [PKCβII]) [5], a tryptophane-aspartate (WD)-repeat protein with multiple potential binding sites that acts as a scaffold in assisting and modulating multiple protein-protein interactions [6, 7].

AChE-R/RACK1 interaction has been revealed in a two-hybrid screen of foetal brain cDNA library and validated by co-immunoprecipitation of both proteins from glioblastoma or AChE-R transfected cells [5]. By binding RACK1, AChE-R recruits PKC, inducing distinct signal transduction pathways in cells of various tissue origins [5, 8, 9]. The normally rare AChE-R variant is induced by chemical, psychological or immunological stressors in brain, muscle, blood and testicular cells alike [10–13]. Parallel increases occur during neuronal and haematopoietic differentiation [12, 14]. Transgenic overexpression of human AChE-R correlated with decreased mouse sperm counts, and AChE-R localization patterns varied between sperm from fertile and infertile men [13]. To explore the cellular processes affected by AChE-R during spermatogenesis, we addressed its protein-protein interactions in the continuously changing settings of male germ cell differentiation.

Materials and methods

Yeast two hybrid screen

Screening involved a testes cDNA library from 19 Caucasians, ages 17-61 that died of trauma (3.5×10^6 independent clones, MATCHMAKER pre-transformed two-hybrid library, Clontech, Mountain View, CA, USA), cloned in the AD pGADT7 vector transformed into yeast Y187 cells. The 'bait' encoding the 53 C-terminal residues of the AChE-R protein (ARP53), 28 of which are unique to this AChE variant cloned in the DNA-BD pGBKT7 vector transformed the AH109 yeast strain [5]. The two strains were mated and diploid cells, representing 7.02×10^6 clones, were plated on minimal medium. Isolated plasmids from positive clones were PCR-amplified and sequenced. Sequences were examined for the presence of an open reading frame and matching Genebank entries (www.ncbi.nlm.nih.gov/BLAST/). The resultant 22 clones were co-transfected with irrelevant Lamin-encoding BD pGBKT7 plasmid, to exclude self-activation of reporter genes. This screen yielded 13 validated positive clones encoding seven different proteins.

Expression and purification of recombinant human RACK1

RACK1 was subcloned by direct recombination, using cDNA received gratefully from Mochly-Rosen [15] into inducible Gateway® pDest14 entry vector (Invitrogen, Carlsbad, CA, USA), overexpressed in BL21-ps$^+$ *E. coli* cells, from nearly undetectable level before induction to 12% of soluble protein in cell homogenates. One-step purification procedure with Q-SepharoseFF anion exchange chromatography yielded 120 mg of 97% pure protein per litre culture, as verified by immunoblots.

Enzyme activity assay

Recombinant hAChE-R was purified from transgenic *Nicotiana benthamiana* (Tobacco) plants [16]. Cholinesterase activity measurement was as described [17]. Prior to addition of substrate, purified AChE-R was incubated with either RACK1, enolase-α (Hytest, Turku, Finland) or with both proteins in assay solutions (10 min., room temp.). Km and Vmax were calculated with Michaelis-Menten equation by KALEIDAGRAPH software (Synergy Software, Reading, PA, USA).

Enolase-α activity was assayed in 0.1M Phosphate buffer pH7.4, 2.7 mM Mg acetate, 1mM EDTA with 3 mM 2-phosphoglyceric acid (2-PGA, Sigma, St. Louis, MO, USA) as substrate. Phosphoenol pyruvate accumulation was measured at 240 nm. Prior to addition of substrate, enolase was incubated (10 min., room temp.) with a synthetic peptides constituting the 26 amino acids-long C-terminal sequence of human AChE-R (ARP26) or 23 C-terminal residues of AChE-S (ASP23) [12].

Co-immunoprecipitation

Testicular tissue of adult TgR mice or strain-matched controls [13] was homogenized in 1M NaCl, 10 mM ethylene glycol tetraacetic acid (EGTA), 10 mM Tris-HCl pH7.4, 1%

TritonX100, incubated on ice 45 min. and centrifuged (15,000 rpm, 1 hr, 4°C). Supernatant protein concentration was determined (DC™ protein assay, Bio-Rad, Hercules, CA, USA) and AChE activity determined [13]. Samples of 500 μg protein were incubated (overnight, 4°C) in 0.5 ml NET buffer [8] containing 0.1% NP-40 and 1 mM EDTA (pH 8.0) with goat anti-AChE N-terminus (SC-6431; Santa Cruz Biotechnology, Santa Cruz, CA, USA), rabbit anti-non-neuronal enolase (NNE) (Biogenesis Ltd., Poole, UK) or biotin-conjugated donkey anti-goat IgG antibodies (Jackson, West Grove, PA, USA), each diluted 1:50 v/v. Protein A or G sepharose beads were added as described [8]. Samples were washed three times with the supplemented NET buffer (1 min. centrifugation, 13,000 rpm), re-suspended in 50 μl sample buffer [5], heated (5 min at 90°C), re-centrifuged as above and supernatant collected. SDS-gel electrophoresis (4–12% Novex® Tris-glycine gradient gel, Invitrogen, Carlsbad, CA or 7.5% ReadyGel® Tris-HCl gel, Bio-Rad) and immunoblotting were essentially as described [5] with either mouse anti-rat RACK1 (BD, San Diego, CA, USA) or anti-human AChE N-terminus. Co-immunoprecipitation on pup (20 days old) testes homogenates, was performed on 750 μg total protein pooled from three animals of each strain as described above in 0.01 M Phosphate buffer pH 7.4 with 4 μg rabbit anti-GNβ2L1 (*i.e.* RACK1, Abgent, San Diego, CA, USA). Immunodetection was performed with mouse anti-RACK1 (BD) 1:1000, mouse anti-TAp73 (IMG-146; Imgenex, San Diego, CA, USA) 1:250, anti-ΔNp73 (IMG-313; Imgenex) 1:350 and anti-α Tubulin (Santa Cruz) 1:2000.

Human and animal tissues

Human testicular biopsies containing normal tissue, obtained during removal of a testicular tumour or biopsies obtained for infertility workup, were formalin fixed and paraffin embedded. TgR mice of the FVB/N strain carry the human AChE-R coding sequence: E2, E3, E4 and I4 and display a Mendelian inheritance pattern [18]. The transgene is regulated by the cytomegalovirus (CMV) minimal promoter and contains the SV40 polyadenylation signal. Transgene presence was PCR verified and transgenic mice were repeatedly mated to ensure homogeneity. Transgenic and control FVB/N mouse pups (≥4 per age group) were sacrificed at noted post-natal day (p.n.d) with day of birth termed p.n.d 1. Adult, 3-month-old mice were used for comparison. Mouse testes were fixed in Bouin`s fixative (75% picric acid, 20% formaldehyde (37%), 5% acetic acid) for 2 hrs, transferred to 70% ethanol and embedded in paraffin. For analysis, 7 μm thick slices were prepared. Ejaculates from human sperm donors and patients with undetermined sperm quality were allowed to liquefy and washed. All patient samples and three donor samples were subsequently frozen. Fresh or thawed sperm samples were centrifuged through a discontinuous 50% and 90% density gradient medium (ISolate®, Irvine Scientific, Santa Ana, CA, USA). Cells in each gradient layer and on top were collected, producing three fractions from each sample. Cells in each fraction were microscopically evaluated and motility assessed according to the World Health Organization (WHO) Manual for the Assessment of Human Semen. Motility grades were termed 1 to 4 corresponding to the A-D scale (1 = D, 4 = A). The institutional review board at the Tel Aviv Sourasky Medical Center and the Hebrew University's authority for animal experiments (permit no. NS-01-29) approved this study.

Immunohistochemistry

Detection of AChE-R was with a polyclonal antibody manufactured against the human C-terminus which also binds mouse AChE-R [14, 19]. Immunostaining with rabbit anti-AChE-R or mouse anti-RACK1 (BD) diluted 1:100 and 1:50 v/v, respectively, was essentially as described [13]. Colorimetric detection involved biotinylated secondary antibodies and the ABC reagent (Vector Labs, Burlingame, CA, USA) with 3, 3′-diaminobenzidine hydrochloride (DAB, Sigma) as substrate. Alternatively, alkaline phosphatase-conjugated secondary antibodies were used with the substrate Fast Red (Roche Diagnostics, Mannheim, Germany). Counterstaining was done with hematoxyline. Human testis immunostaining was scanned with an Olympus FV100 confocal microscope equipped with an IX81 inverted microscope using 40×/0.6 N.A. objective. Excitation wavelength was 488 nm and emission collected using 560-620 nm filter; DIC images were collected simultaneously. A confocal plane was scanned every 0.5 μm and a three-dimensional projection created from all sections. Mouse testis immunostaining was viewed with Zeiss Axioplan microscope (Zeiss, Göttingen, Germany) using 40×/0.75 objective and captured with Real-14™ digital colour camera (CRi, Boston, MA, USA).

Apoptosis assay

ApoAlert™ DNA Fragmentation Assay Kit (BD), served to quantify apoptotic cells in pup testicular sections from p.n.d 18–20, by TUNEL reaction. Additionally, 4′,6-diamidino-2-phenylindole (DAPI) staining revealed nuclear morphology for apoptosis determination. Nuclei stained for fragmented DNA were counted in at least two separate sections per testis. Proliferating cell nuclear antigen (PCNA) immunostaining and DAPI nuclear staining of adult testes sections were as detailed [13].

Cell culture and transfections

CHO and HEK-293 cells were grown at 37°C, 5% CO_2 in Dulbecco's modified Eagle's medium (DMEM) containing L-glutamine (Sigma) supplemented with 10% foetal calf serum. For glucose uptake assay, cells were transfected with expression plasmids encoding AChE-R, AChE-S [20] or green fluorescent protein (GFP) under cytomegalovirus (CMV) promoter (pEGFP-C2; Clontech) using Lipofectamine^{TM} 2000 (Invitrogen) and assayed the following day. For adenosine tri-phosphate (ATP) assay, CHO cells were stably co-transfected with AChE encoding plasmid and pEGFP-C2 which contains GFP and G-418 resistance gene in 1:10 molar ratio. Cells were selected for approximately 21 days with 500 μg/ml G-418. Surviving colonies were pooled and grown in medium supplemented with 200 μg/ml G-418.

Glucose uptake

CHO and HEK-293 cells were grown in 12 and 24 well plates at 2–4 $\times$ 10^5 and 1 $\times$ 10^5 cells per well, respectively. Medium was removed 24 hrs after transfection, plates washed with phosphate-buffered saline (PBS) and cells incubated in serum-free DMEM containing 4.5 mg/ml glucose (Sigma) for 3–4 hrs. Glucose concentration in medium diluted in double-distilled water was calculated from a standard curve (Glucose [HK] Assay kit, Sigma). Medium incubated in wells without cells served as baseline control.

Cellular ATP levels

Mouse cauda epididymis was shredded in 150 mM NaCl, 5.5 mM KCl, 0.4 mM $MgSO_4$, 1 mM $CaCl_2$, 10 mM NaHCO3, 4-(2-hydroxyethyl) piperazine-1-ethanesulfonic acid (HEPES)-NaOH pH7.4 and 5 mM glucose; allowed to sink for about 1 min., and cell suspensions transferred to clean tubes. Assay was performed essentially as described elsewhere [21] by a luciferase bioluminescence assay (ATP Bioluminescence Assay kit CLSII; Roche).

Mouse sperm motility measurements in CASA device

Sperm cells (1 $\times$ 10^7 cells/ml) were incubated for 5 min. in HEPES medium bicarbonate (HMB) medium [22]. Samples (5 μl) were placed in standard count 4 chamber slide (Leja, Nieuw-Vennet, Netherlands) and analysed by computer-aided sperm analysis (CASA) device with IVOS software (version 12, Hamilton-Thorne Biosciences, Beverly, MA, USA). Up to 10 sequels, 30 sec. long were acquired for each sample. Cells were analysed according to parameters identifying mouse sperm motility. The proportion of hyperactivated spermatozoa in each sample was determined using the SORT function. Hyperactivated motility was defined by curvilinear velocity (VCL) >90 μm/s, linearity (LIN) <20% and amplitude of lateral head (ALH) >7 μm. Percentage of hyperactivated cells was calculated out of overall motile cells.

JC1 staining

Mouse cauda-epididymis was shredded in 1 ml of HEPES/bovine serum albumin (BSA) buffer [23], allowed to sink for about 1 min., and cell suspensions transferred to clean tubes. Aliquots (200 μl) were incubated with 3 μM JC1 (5,5′,6,6′-tetrachloro-1,1′,3,3′-tetraethylbenzimidazolyl-carbocyanine iodide, Molecular Probes) and 12 μM PI (Sigma, 20 min., room temp), centrifuged (500 g, 7 min.) to remove excess dye, placed on glass slides, covered with coverslips and examined by confocal microscopy. Viable motile cells that reached the drop's periphery were subjected to quantitative evaluation of JC1 staining. Fluorescence was measured with an MRC-1024 BioRad (Hemel Hempsted, Hertfordshire, U.K.) confocal microscope equipped with an inverted microscope using a 40×/1.3 oil immersion objective. Excitation was at 488 nm and emission measured at 525 ± 40 nm (green) and 585lp nm (red). Propidium iodide (PI) fluorescence was measured with 655±90 filter. The ratio between red and green fluorescence intensity was calculated [23]. Cells with compromised membrane integrity (reflected by PI nuclear staining) were excluded.

Immunocytochemistry for microscopic analysis

Analysis was performed on sperm cells from TgR epididymis shredded in saline and from liquefied human ejaculates washed in PBS. Free cells were smeared on Superfrost® Plus glass slides (Menze-Gläser, Braunschweig, Germany), allowed to air dry then treated with 70% ethanol. Mouse and human sperm cells were immunostained for AChE-R (1:100) [19]. Biotinylated secondary antibodies were detected by confocal microscopy with streptavidin conjugated to Cy2 (Jackson Laboratories) or alkaline phosphatase using Fast Red (Roche) as substrate. Negative control staining for human cells was without primary antibody. Confocal microscope settings were as listed for JC1 detection except emission was measured at 525 ± 20 (Cy2) or 580 ± 16 (Fast Red). A confocal plane was scanned every 0.5 μm and a three-dimensional projection created from all sections using the ImagePro Plus software (Media Cybernetics, Silver Spring, MD, USA).

Cell stains for flow cytometric analysis

A sample of each density gradient fraction was washed in nine volumes of PBS and diluted to 5×10^6 cells/ml. Cells were incubated (20 min. on ice) with 0.05 mg/ml propidum iodide solution [24] 1:1, v/v. Aliquots of 1×10^6 cells were centrifuged (10 min., 500×*g*). Cells were suspended in 50 µl PBS, incubated (30 min., 4°C) with 4 µl of rabbit anti-AChE-R or anti-NNE, washed with 1ml PBS, incubated with 3 µl of fluorescein isothiocyanate (FITC)-conjugated goat anti-rabbit IgG (Zymed, San Francisco, CA; 30 min., 4°C) in 50 µl, washed, re-suspended in 200 µl PBS and analysed by flow cytometry.

Flow cytometric acquisition and analysis

Four-parameter, 2-colour flow cytometry used a BD FACS Calibur to acquire 20,000 events per sample. Compensation was adjusted for both fluorescence parameters. Cell Quest and Cell Quest Pro software (BD) were applied for data analysis. All files were saved as list mode data.

Results

AChE-R interacts with both RACK1 and enolase

A cDNA expression library from adult human testis (3.5×10^6 clones) was screened with the C-terminal region of human AChE-R (ARP-53) as 'bait' [5] (Fig. 1A). This yielded 13 independent clones reflecting partner protein interactions. Four of the identified clones included RACK1 sequences spanning most of the coding sequence, including WD domains 5–6 shown to interact with AChE-R in neurons [5] (Fig. 1B). A single enolase-α encoding clone covered 49% of the coding region, spanning its active site (Fig. 1B).

To test whether intact AChE-R interacts with RACK1 and enolase, we evaluated AChE's biochemical properties as an indication for protein–protein interaction [25]. Highly purified recombinant human AChE-R (hAChE-R) expressed in *Nicotiana benthamiana* plants [16] was incubated with stoichiometric amounts of purified recombinant RACK1 and purified enolase-α. This elevated AChE-R's cholinesterase activity (Fig. 1C). That incubation with RACK1 and enolase-α together did not produce an increased activation suggests that all AChE units were fully engaged at the 1:10 molar ratio. Acetylthiocholine hydrolysis tests demonstrated that AChE-R maintained its Km in the presence of RACK1 or enolase (46 ± 5 *versus* 48 ± 9 or 55 ± 5 µM respectively), indicating that the affinity of the enzyme to its substrate was unchanged; however, Vmax was increased by the interaction (12.6 ± 0.3 *versus* 15.0 ± 0.5 or 15.0 ± 0.3 arbitrary units/min; Fig. 1C), demonstrating that protein interaction with either partner had a similar enhancement on the catalytic turnover.

To validate AChE-R interactions in the testis, we co-immunoprecipitated RACK1 and enolase-α from testicular homogenates of transgenic TgR mice overexpressing hAChE-R in primary spermatocytes, elongated spermatids and spermatozoa [13]. Antibodies to the AChE common domain, but not non-specific rabbit immunoglobulins, co-precipitated a 36KD protein recognized by antibodies to RACK1 (Fig. 1D). Antibodies to RACK1 did not interact with the precipitating antibody, attesting to the specificity of this precipitation. Reciprocally, antibodies to non-neuronal enolase co-precipitated 60 and 66KD proteins, recognized by the anti-AChE antibodies (Fig. 1D). We conclude that, in testicular mouse tissue, AChE-R can form complexes with both RACK1 and enolase-α.

Developmentally modified distribution of spermatogenic AChE-R and RACK1

Prior to our current study there was no evidence attesting to the fact that RACK1 is expressed during spermatogenesis. Rather, RACK1 protein has only been detected in bovine-ejaculated sperm [26]. Immunohistochemistry showed cytoplasmic AChE-R and RACK1 labelling in human testicular sections containing all spermatogenic stages, but non-specific rabbit immunoglobins showed no notable labelling (Fig. 2A). Cytoplasmic droplets to be removed from spermatozoa as residual bodies, were intensively stained for AChE-R (Fig. 2A, inset). To study the impact of AChE-R on spermatogenesis, we used AChE-R overexpressing TgR mice as a model. In pre-pubertal TgR pups, AChE-R labelling was confined to meiotic spermatocytes and could only be detected from p.n.d 14 (Fig. 2B8-11), indicating null expression in spermatogonia and somatic Sertoli cells (Fig. 2B7). In adult TgR testis, AChE-R staining

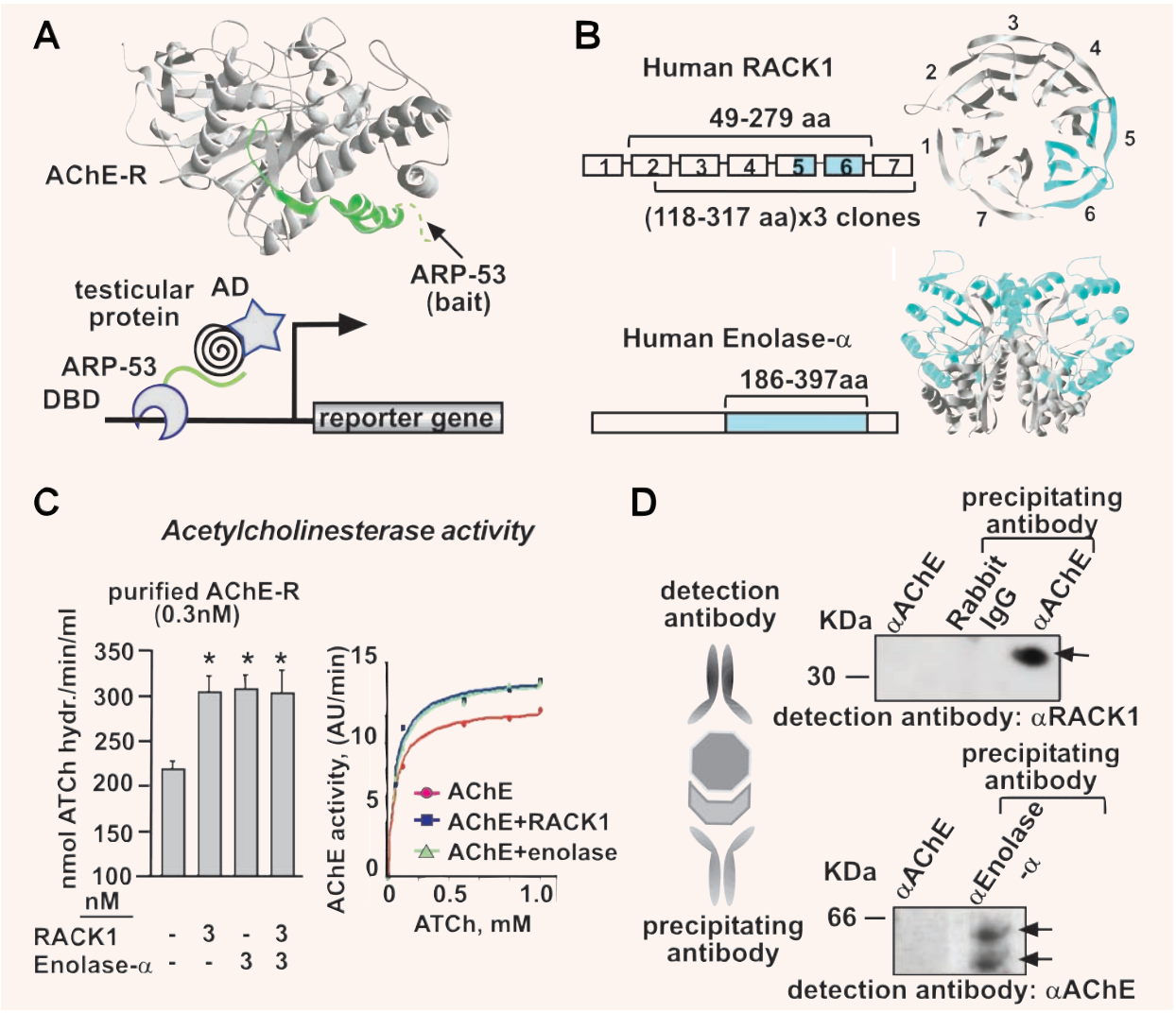

Fig. 1 Testicular AChE-R interacts with RACK1 and enolase-α. (**A**) Yeast two hybrid screen. DNA encoding for the C-terminal domain of AChE-R (ARP-53, green [5]) was fused to the DNA-binding domain (DBD) of the GAL4 transcription factor. Human cDNA library encoding testicular proteins fused to the GAL4 activation domain (AD) was screened for restored GAL4 function, enabling transcription of several reporter genes. (**B**) RACK1 and enolase-α interaction domains. Top: four clones encoding RACK1's WD domains 2–6 out of its 7, including the region interacting with brain-AChE-R (blue). RACK1 model follows the homologous G-protein β1 subunit (PDB ID: 1GP2), localized region of AChE-R interaction shaded in blue. Bottom: One clone of enolase-α that spanned half of this protein, highlighted (blue) in the crystal structure of the enolase homodimer (PDB ID: 1EBH). (**C**) Both RACK1 and enolase-α affect AChE-R activity. Incubation with enolase-α or RACK1 increased recombinant AChE-R ability to hydrolyse acetylthiocholine (Average values ±S.E.M, $n = 6$; *$P<0.01$, Student's t-test). Plots: Substrate hydrolysis rate by 0.3 nM recombinant AChE-R was measured at indicated acetylthiocholine concentrations to determine the effect of RACK1 and enolase binding on AChE-R activity. Plot was drawn according to the Michaelis-Menten equation. (AU, arbitrary units). Note increased Vmax in presence of both binding partners [50]. (**D**) Co-immunoprecipitation validates AChE-R interactions. Testicular homogenates from TgR mice were incubated with the noted precipitating antibodies and electroblotted. Immunolabelling detected RACK1 (36 KD) in anti-AChE but not IgG precipitates. Two proteins (66 KD and 60 KD) immunopositive with anti-AChE antibodies were co-precipitated by anti-enolase-α. Anti-AChE immunoglobulins (negative control) yielded no labelling at these sizes.

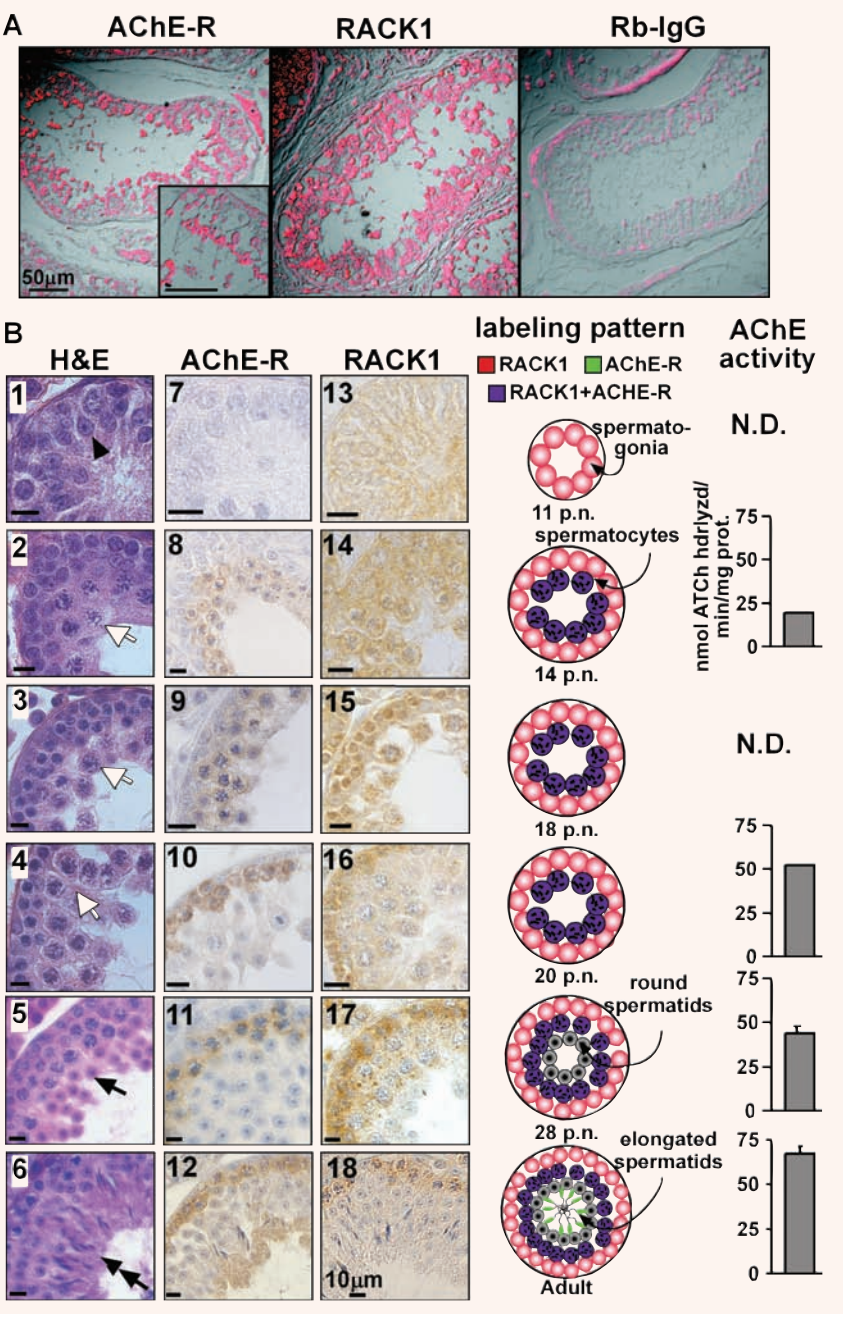

Fig. 2 Developmental co-localization of RACK1 with testicular AChE-R. (**A**). Seminiferous tubules from healthy human testis. Both RACK1 and AChE-R are immunodetected in spermatogenic cells. AChE-R could also be detected in intratubular tissue. Unspecific rabbit immunoglobulins (RbIgG) did not yield any notable staining. Inset: Higher magnification of testicular spermatozoa, note cytoplasmic staining. (**B**). Developing mouse testis. β1–6: Representative seminiferous tubules of newborn TgR mice with spermatogonia germ cells (black arrowhead), meiotic spermatocytes (days 14–20, white arrow), haploid round spermatids (black arrow, day 28), elongated spermatids (adult, double arrow). B7–12: AChE-R in meiotic spermatocytes and in elongated spermatids at spermatogenic stages I-VI. B13–18: RACK1 in spermatogonia and in meiotic spermatocytes. Drawings: Cell layers in seminiferous tubules during progressing spermatogenesis, co-localization of AChE-R (green) and RACK1 (red) is indicated (purple). Levels of AChE activity in testicular homogenates are presented. H&E, haematoxylin-eosin staining; N.D., not determined.

could also be detected in cytoplasm of the more advanced elongated spermatids (Fig. 2B12), indicating high levels of AChE-R in late stages of spermatogenesis and resembling the staining pattern in human tissue. RACK1, however, could be detected already at p.n.d 11 when, apart from Sertoli cells, only the germline stem cells, spermatogonia, are present in the tissue (Fig. 2B1 and B13).

Diffusely distributed cytoplasmic RACK1 staining was apparent in spermatogonia at all ages examined. At p.n.d 14, diffuse RACK1 staining could be detected in early meiotic spermatocytes (Fig. 2B14). By p.n.d 18 (Fig. 2B15), focal RACK1 aggregations appeared in spermatocyte cytoplasm; and at p.n.d 28 (Fig. 2B17, Fig. 3A), cytoplasmic RACK1 staining became completely focal. Round haploid spermatids,

also visible at p.n.d. 28 (Fig. 2B5), did not display RACK1 staining at all, indicating developmental regulation of expression and of intracellular localization of RACK1 during sperm differentiation. Reduced RACK1 transcripts in mouse round spermatids as compared with preceding steps of spermatogenesis was also reported in microarray studies [27]. RACK1 immunostaining patterns were similar in the FVB/N parent strain (data not shown), excluding the possibility of transgenic-induced changes. In adult testis cross-sections, RACK1 was detected at all spermatogenic stages whereas AChE-R expression appeared in spermatocytes at stages I–VI of the spermatogenic cycle. AChE activity in the testicular homogenates from TgR pups normalized per total protein content presented an age-dependent increase attesting to the rising number of AChE expressing cells as spermatogenesis progresses. No activity could be detected in control mice (data not shown). In mouse but not human tissue, RACK1 and AChE-R were both undetectable following the transition from meiotic spermatocytes to haploid spermatids (Fig. 3A), suggesting protein degradation. The co-localization of RACK1 and AChE-R in spermatocytes and the precipitation of AChE-R/RACK1 complexes from TgR testicular homogenates predicted that these complexes form in spermatocytes.

Increased apoptosis in spermatocytes of TgR mice

To reveal the consequences of AChE-R/RACK1 interaction in spermatocytes, we counted spermatogonia and spermatozoa, the cellular stages preceding and following meiosis, in seminiferous tubule cross-sections from adult mouse testis. Cell counts normalized per tubule perimeter revealed similar contents of the AChE-R-null spermatogonia stem cells; however, contents of late spermatids were significantly lower in TgR mice as compared with controls (Fig. 3B). Correspondingly, transgenic pups displayed elevated spermatocyte apoptosis as measured by TUNEL staining of testicular sections at p.n.d 18–20, an age when spermatocytes are the majority of the germ cell population and undergo extensive apoptosis [28] (Fig. 3C). Additionally, TgR mice display lower epididymal sperm concentration than strain-matched controls or TgS transgenic mice overexpressing the synaptic AChE-S variant (3.9 ± 0.4 *versus* 6.45 ± 0.7 or $5.3 \pm 1.2 \times 10^6$ cells/ml, respectively [13]), supporting the notion that the unique C-terminus of AChE-R is involved. We thus examined the effect of AChE-R overexpression on RACK1 interaction with p73α, a transcription factor expressed in spermatocytes [29]. p73α, can have either pro- or anti-apoptotic function depending on the inclusion of a trans-activation domain, which is not involved in RACK1 binding [30].

RACK1 concentration was similar in testicular homogenates from TgR pups at p.n.d. 20 as compared with control pups; this was also the case for TAp73 (total protein, Fig. 3D). Nevertheless, RACK1 precipitates from TgR testes pulled down less TAp73 than control homogenates (RACK1 i.p., Fig. 3D), suggesting larger amounts of TAp73 remained free. Supporting this notion, TgR homogenates showed elevated levels of ΔNp73, known to be induced by TAp73, which also co-precipitated with RACK1 (RACK1 i.p., Fig. 3D). The increase in RACK1/ΔNp73 was proportional to the increase in the total level of this protein. However, tubulin levels remained unchanged (data not shown). With less TAp73 inactivated by RACK1, TgR spermatocytes should experience more p73-dependent, pro-apoptotic events then spermatocytes of control mice. However, further experiments and molecular analysis are required to verify that AChE-R can promote apoptosis *via* TAp73.

AChE-R and its C-terminal peptide, ARP26, enhance enolase activity glucose uptake and ATP levles

Enolase, a key enzyme of the glycolytic pathway, is active as a homo- or hetero-dimer formed from three highly similar isoenzymes (α, β and γ). Enolase-β and -γ are predominantly expressed in muscle and neuronal cells, respectively, but enolase-α is a ubiquitous protein found in a variety of tissues [31], spermatogenic cells included [32]. The enzymatic activity of purified enolase-α was tested *in vitro* in the presence of synthetic ARP26 or ASP23, the C-terminal peptides of human AChE-R or AChE-S [12] (Fig. 4A). ARP26, but not ASP23, elevated enolase-α activity by 34% (Fig. 4B), supporting the notion that the ARP domain suffices to modify the biochemical properties of AChE-R/enolase-α complexes. Moreover, in the enolase-expressing CHO and HEK293 cells, hAChE-R but not hAChE-S transfection increased glucose

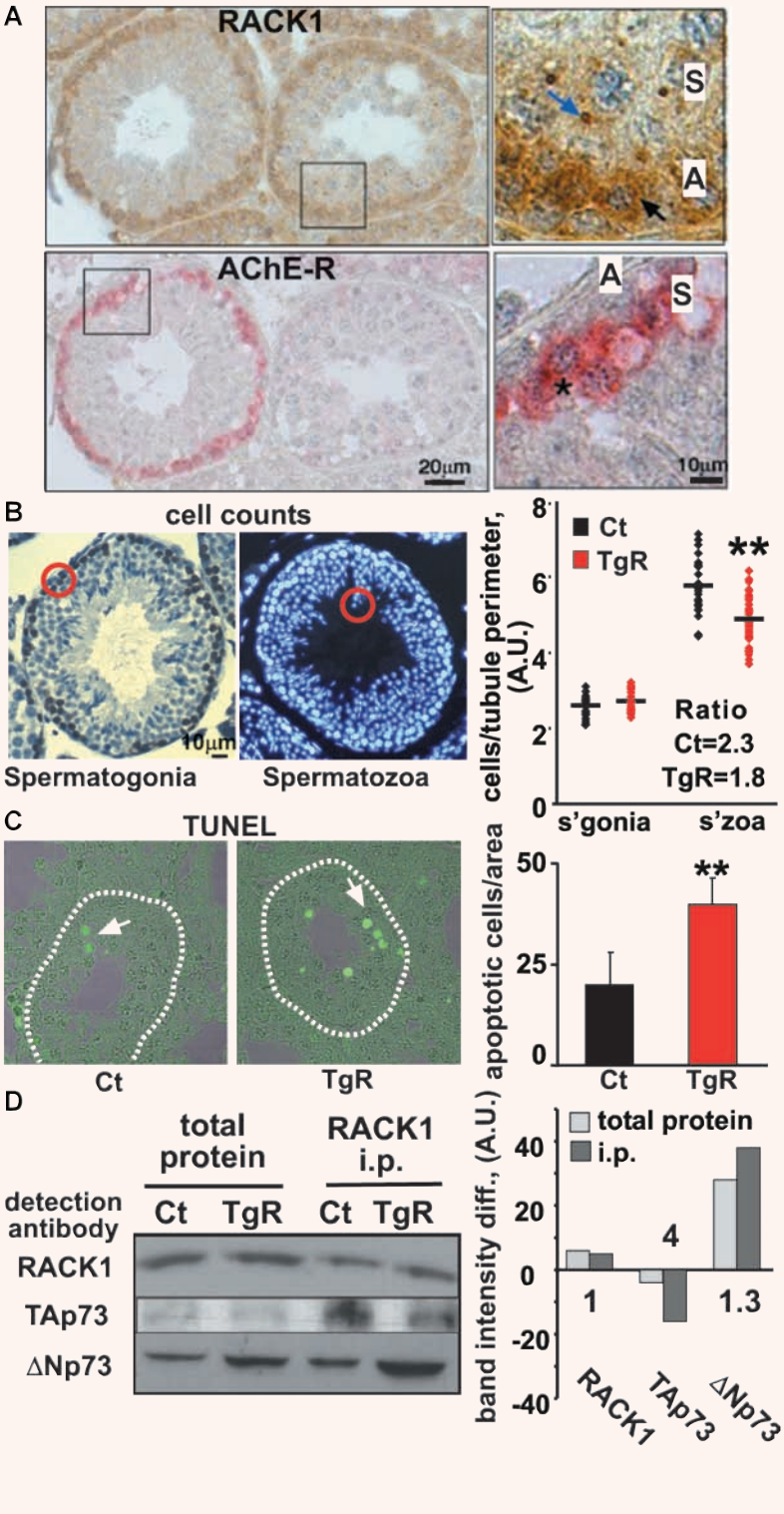

Fig. 3 Apoptosis of meiotic spermatocytes under AChE-R/RACK1 displacement of TAp73 (**A**). AChE-R and RACK1 co-expression in meiotic spermatocytes of TgR mice. Immunostaining in consecutive testicular sections of adult mice. RACK1 is expressed in spermatogonia (A, black arrow), which lack AChE-R, and forms foci in meiotic spermatocytes (S, blue arrow), which express AChE-R with both focal (*) and diffuse localization. Squares mark areas of higher magnification. (**B**). Reduced sperm production in TgR mice. Numbers of spermatogonia immunostained by proliferating cell nuclear antigen (PCNA) and DAPI-stained spermatozoa (red circles) were normalized per tubule perimeter (arbitrary units, A.U.; 10 random tubules per animal, 2–4 animals per group). A significant decline in testicular spermatozoa counts occurred in TgR mice as compared to controls (Ct, $^{**}P<0.001$, Student's t-test). Ratio of spermatogonia to spermatocyte counts is presented. (**C**). Elevated apoptosis in TgR pups. Shown are average numbers of TUNEL-stained cells normalized per tissue area (±S.E.M) in testicular sections from 20-day-old pups, when spermatocytes are the main population in the seminiferous tubule (2–4 sections per mouse, three mice per strain, two independent experiments). Representative tubules from control and transgenic tissues, arrows mark stained cells ($^{**}P<0.001$, Student's t-test). (**D**). Reduced RACK1/TAp73 complexes in 20-day-old TgR pups. Pooled testicular homogenates from three TgR or control (Ct) pups were precipitated with anti-RACK1 polyclonal antibody. Homogenates (total protein) and precipitates (RACK1 i.p.) were electroblotted with noted detection antibodies. Bar graph presents the ratio between band intensity of TgR and control samples. Numbers note fold difference.

uptake by two fold (compared to GFP-transfected cells as a negative control (Fig. 4C)). Enolase activity can affect glycolytic rate and cellular ATP levels [31, 33], although *in vitro* this activity is at equilibrium. Importantly, ATP levels were also increased in CHO cells stably expressing hAChE-R but not hAChE-S (Fig. 4D), anticipating that AChE-R overexpression can potentially accentuate glycolysis and ATP content in sperm cells as well.

Increased ATP levels and mitochondrial depolarization in AChE-R transgenic sperm

To determine the glycolytic rate of transgenic sperm, the ATP content of TgR and control epididymal sperm was measured. Over 3.5-fold elevation in ATP levels was observed in TgR sperm as compared with control (Fig. 4D). Immunocytochemistry of mouse and human sperm cells detected AChE at the midpiece and principal piece, the site of the sperm mitochondrial sheath and glycolytic machinery (Fig. 4E and F), thus placing AChE at a location where it can directly affect glycolytic enzymes. In sperm cells, glycolytic activity and ATP levels correlate with motility [21]. This raised the possibility that sperm motility in TgR mice is also elevated. While insufficient to maintain cellular ATP levels, mitochondrial activity is a reliable measure of sperm motility [21, 23]. To test AChE-R effects, enriched viable mouse epididymal sperm cells from TgR and control mice were incubated with the fluorogenic agent JC1 and the DNA-binding agent PI. JC1 fluorescence shifts from green to red, under mitochondrial membrane hyperpolarization (Fig. 4G). Freely swimming sperm cells were refractory to PI staining, indicating cell membrane integrity (Fig. 4G). Compound confocal images of PI-impermeable individual sperm cells were subclassified as per their red/green JC1 intensity ratios. The majority of FVB/N sperm cells displayed 1.2–1.6 ratios as compared with 1.6–2.2 ratios in TgR cells, demonstrating mitochondrial hyperpolarization under AChE-R overexpression (Fig. 4H). Epididymal sperm of TgR mice further displayed elevated overall motility compared with controls as determined by computer-assisted sperm analysis (CASA) measures (Fig. 4I). Moreover, TgR sperm contained more cells presenting hyperactivated motility (Fig. 4I), characterized by elevated flagellar beating, which presents greater ATP demands [34].

Sperm motility in human donors, but not infertility patients correlates with AChE-R labelling

To test the implications of AChE-R interactions on human sperm motility, we used density gradient centrifugation of ejaculates to subclassify sperm into three cell populations. Cells were immunostained for AChE-R and enolase-α, and the fluorescent signals in gated sperm cells, as detected by flow cytometric analysis [24], were compared with those of unstained cells (Fig. 5A). Overall motility and quality of movement were microscopically determined for each subpopulation (Fig. 5B). Expectedly, enriched normal sperm (fraction I) from both sperm-bank donors and patients were significantly more motile and with increased forward movement compared with sperm cells from the fraction of lowest density (fraction III; Fig. 5B). Moreover, donor sperm samples (both fresh and frozen) were significantly more motile than patient samples in all fractions. Density gradient selection yielded a significant increase in AChE-R positive cells in donors but not patients (Fig. 5C), with a twice-higher fraction I/III ratio (2.71 ± 0.28 *versus* 1.27 ± 0.17 s.e.m, $P = 0.004$, Student's t-test). Also, highly motile donors' sperm (fraction I) showed higher proportion of AChE-R positive cells than in patients ($71\% \pm 6.3$ *versus* $43\% \pm 7.4$ S.E.M.). Enolase-α however, was similar in donors and patients or between gradient fractions (Fig. 5C), indicating causal relationship between AChE-R, but not enolase-α protein content, and sperm motility.

Discussion

Our two-hybrid screen demonstrated that the C-terminus of AChE-R enables the formation of complexes with the scaffold protein RACK1 and the glycolytic enzyme enolase. While computer modelling cannot exclude the possibility of complexes containing all three proteins (Fig. 6A), the existence of such trimers remains to be demonstrated. At an early stage of spermatogenesis, AChE-R/RACK1 interaction could release TAp73 and induce apoptosis of spermatocytes,

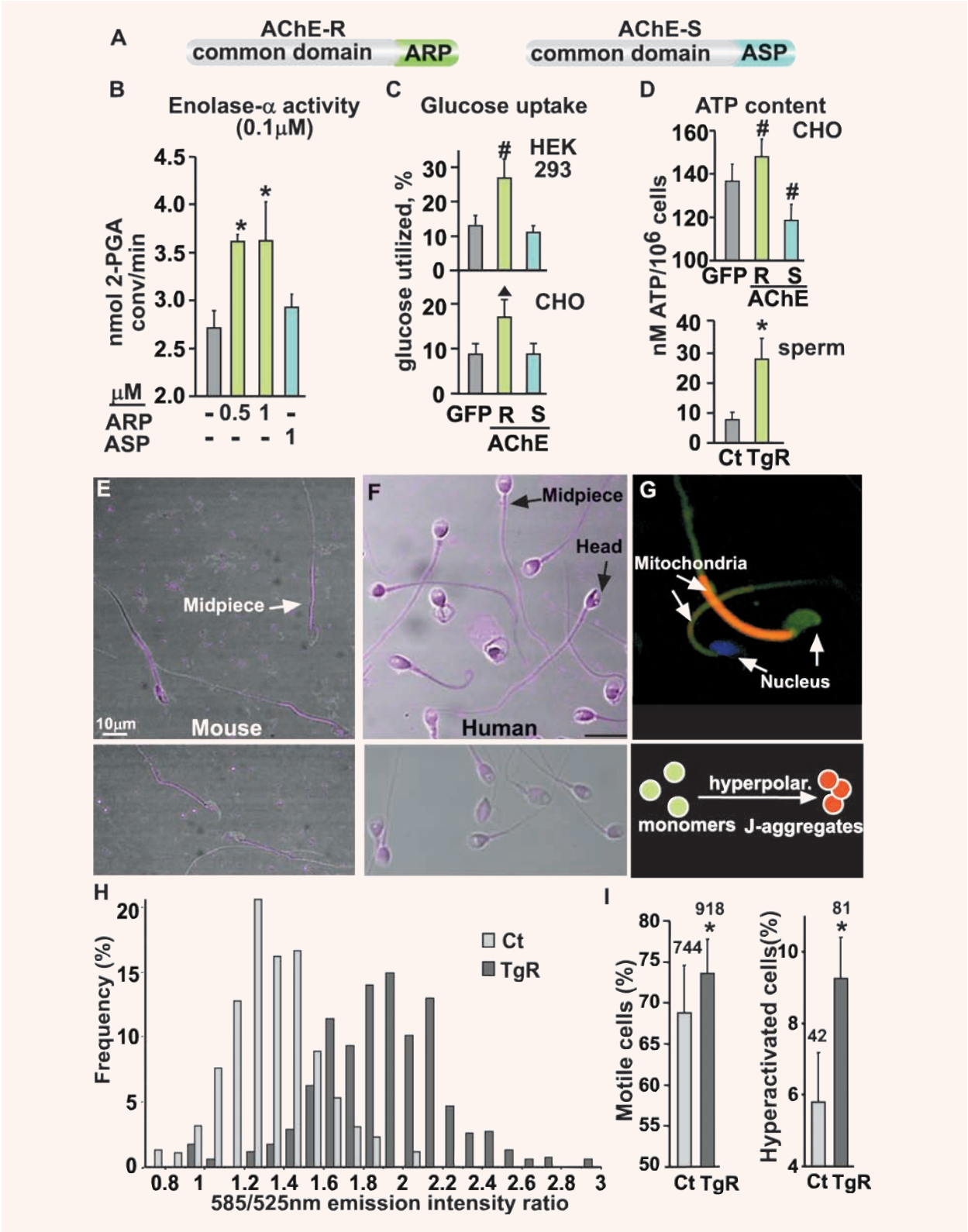

Fig. 4 AChE-R overexpression increases glycolysis in transfected cells and mitochondrial activity in epididymal sperm. **A**. Schematic representation of AChE isoforms. AChE-R and –S are 95% identical, but each isoform contains a unique C-terminus. ARP- AChE-R peptide; ASP - AChE-S peptide. **B**. ARP, but not ASP increases enolase-α activity. Incubation with synthetic ARP26 at a 1:5 or 1:10 enolase:ARP ratio but not with 1:10 synthetic ASP23 increased the hydrolytic activity of purified enolase by 34%. Shown are average values ±S.E.M; **P*<0.05, Mann-Whitney test (*n* = 3). **C**. AChE-R but not AChE-S increases glucose uptake by transfected cells. Shown is glucose uptake from the medium by CHO and HEK293 cells transfected with expression vectors encoding AChE-R, AChE-S or GFP, all with the CMV promoter. Shown are average values ±S.E.M., *P*<0.05, Δ*P*=0.06, one tailed Student's t-test, (*n* = 4–7). **D**. Increased ATP levels in AChE-R overexpressing epididymal sperm cells. ATP was extracted and measured by biolouminescence assay from CHO cells stably transfected with expression vectors encoding AChE-R, AChE-S or GFP (*n* = 5) and from epididymal sperm of TgR and control mice (*n* = 11). Average values ±S.E.M; **P*<0.05, Student's t-test, #*P*<0.05 one tailed Student's t-test. **E**. AChE-R in TgR epididymal sperm. Upper panel: Immunodetection yielded staining in the midpiece and principal piece regions. Lower panel: Only faint staining is visible in non-transgenic mice. **F**. AChE-R in human sperm. Staining in the midpiece and head regions. Lower panel: faint negative control staining. **G**. JC-1 aggregates in mouse epididymal sperm. JC-1 monomers emit green fluorescence; J-aggregates formed by mitochondrial membrane hyperpolarization emit red fluorescence. The red to green fluorescence ratio serves as a measure of mitochondrial hyperpolarization. Mitochondria of cells with compromised membranes, indicated by nuclear staining with propidium iodide (PI, blue), were stained green with JC-1. Live sperm cells with an intact membrane and no PI staining display both green and red (J-aggregates) mitochondrial fluorescence. Merged staining is orange. **H**. Mitochondria hyperpolarization in TgR epididymal sperm. Distribution of red to green fluorescence intensity ratios in 40–45 progressively motile cells per animal (three TgR, four controls). Note greater hyperpolarization in TgR mice (*P*<0.001, Student's t-test). **I**. Elevated overall and hyperactivated motility in TgR epididymal sperm. Shown are percent motile and hyperactivated sperm cells measured by computer-aided sperm analysis (CASA) device. Number of cells for each category is noted. Average values ±S.E.M; **P*<0.05, paired Student's t-test (five control and seven TgR mice).

thus reducing sperm counts. At a later stage in spermatogenesis, AChE-R/enolase interaction likely elevates glucose metabolism, increasing ATP levels and the motility of mature spermatozoa. Thus, by alternating its protein partners, AChE-R affects completely different cellular processes as spermatogenesis unfolds.

AChE-R partner interactions contribute to cellular features

The function of a particular protein is mediated through its choice of partners, and a specific protein can participate in alternating and even opposing cellular pathways. For example, tumour necrosis factor (TNF) receptor 1 can recruit either the apoptosis-inducing TRADD, an activator of Caspase3, or the NF-κB activator, TRAF2, which suppresses apoptosis [35]. The haematopoietic Src family kinase, Hck, activates caspase-induced apoptosis by interacting with the guanine nucleotide exchange factor C3G [36] but is also required for Il-6-induced cell proliferation [37]. In developing male germ cells, we found AChE-R to participate in independent cellular mechanisms of distinct nature, each relevant at a different stage of spermatogenesis and each with a different spermatogenic consequence.

AChE-R/RACK1 interaction may induce p73-mediated apoptosis

RACK1, which displayed spermatogenic-stage dependent subcellular distribution and degradation, represents a junction of many cellular pathways. It has previously been demonstrated to limit stress-induced apoptosis through interactions with numerous contributing proteins [38]. Of these, one putative pathway involves inactivation of the pro-apoptotic transcription factor TAp73 (Transcription Activator p73) [30]. A p53 homologue, TAp73 recognizes regulatory sequences in promoters of pro-apoptotic genes. TAp73 likely affects development, not tumourogenesis [39]. TAp73 also induces transcription from an alternate promoter, yielding an N-terminally truncated dominant-negative protein (ΔNp73) in a negative feedback mechanism to fine tune protein activity levels [40]. By binding the C-terminal sequence unique to the p73α splice-variant, RACK1 prevents TAp73α-dependent transcription and

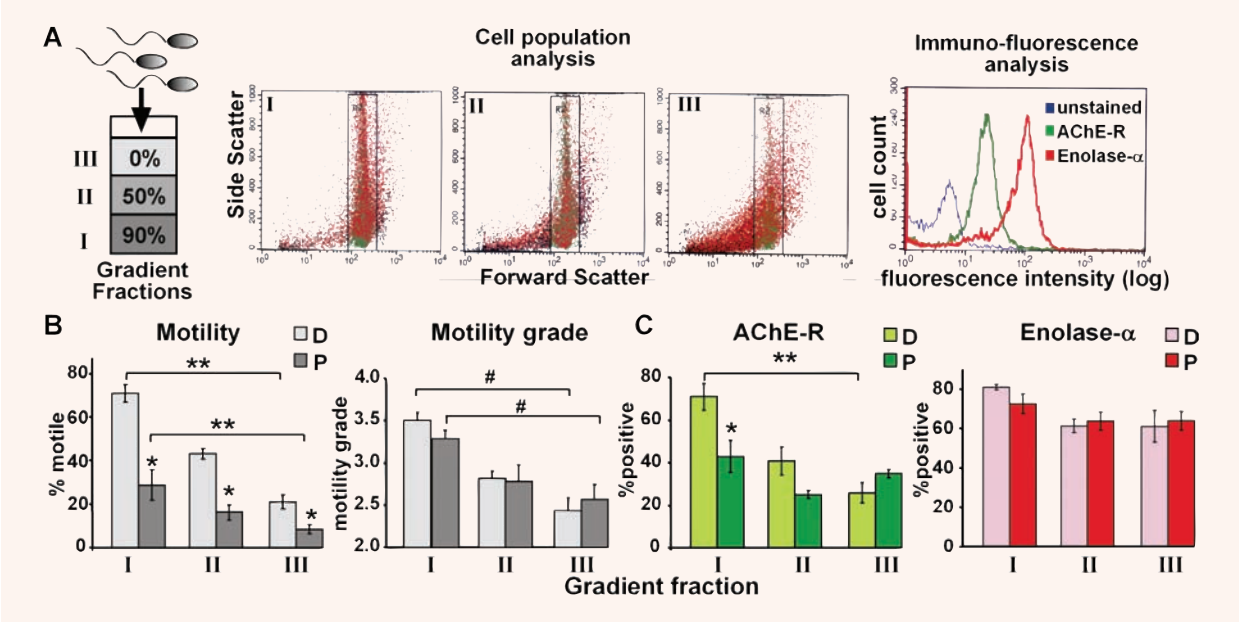

Fig. 5 Elevated AChE-R but not enolase-α in highly motile human donor sperm. **A**. Flow cytometry of human sperm fractions. Sperm samples (donors, $n = 11$; patients, $n = 8$) were subjected to 50–90% discontinuous density gradient fractionation (scheme). Selected sperm (I), intermediate quality sperm (II) and depleted sperm fraction (III) were subjected to flow cytometry. Spermatozoa gate is marked (scatter plots, rectangle). Note sperm enrichment with increasing medium density. Shown is a representative histogram of anti-AChE-R or anti-enolase-α FITC immunofluorescence in comparison with background fluorescence in unstained negative controls. **B**. Selected sperm displays elevated motility. Percentage of motile sperm and quality of movement microscopically determined in donors (D) and patients (P). (Average values ±S.E.M., $^{**}P<0.01$, paired one tailed Student's t-test; $^{*}P<0.01$, Student's t-test; $\#P<0.01$, one tailed Mann-Whitney test.) **C**. AChE-R and enolase-α values. AChE-R, but not enolase-α labeling, was correlated with sperm motility. (Average values ±S.E.M., $^{**}P<0.001$ paired Student's t-test. $^{*}P<0.05$ Student's t-test).

limits apoptosis [30]. Similar to RACK1 and AChE-R (Fig. 3A), p73α is known to reside in peri-nuclear foci in meiotic spermatocytes [29]. The RACK1 region required for p73α binding overlaps the region interacting with AChE-R [5, 30], indicating that these two proteins could compete for the same RACK1 binding site.

In human spermatogenic cells and TgR spermatocytes, AChE-R and RACK1 displayed overlapping localization patterns; both proteins co-precipitated from TgR testis homogenates. While protein extracts were not obtained from isolated spermatocytes, co-immunoprecipitation results suggested that AChE-R/RACK1 complexes originated from this cell type. We therefore regarded TgR mice as a reliable model to examine the consequences of AChE-R imbalance on sperm differentiation.

RACK1/TAp73 complexes were less frequent in transgenic pups, even though the total level of both proteins did not vary between TgR and control mice in protein homogenates. This suggests that AChE-R competition with p73α on RACK1 interactions results in higher levels of free, transcriptionally active TAp73. Correspondingly, this could lead to increased synthesis of the dominant negative ΔNp73 [40], as was indeed observed in TgR testis homogenates. This tilts the balance in meiotic spermatocytes towards apoptosis, thus decreasing their chances to complete spermatogenesis in spite of normal numbers of mitotic spermatogonia. Indeed, TgR but not TgS mice show lower sperm counts, further attributing this phenotype to interactions unique to AChE-R. Interestingly, before this study was initiated, an additional TgR line has been lost due to lack of procreation, supporting the notion that the TgR phenotype is not due to transgene positional effect. That AChE-R inversely exerts proliferative effects in hematopoietic cells [9, 12] highlights the cell context-dependence of

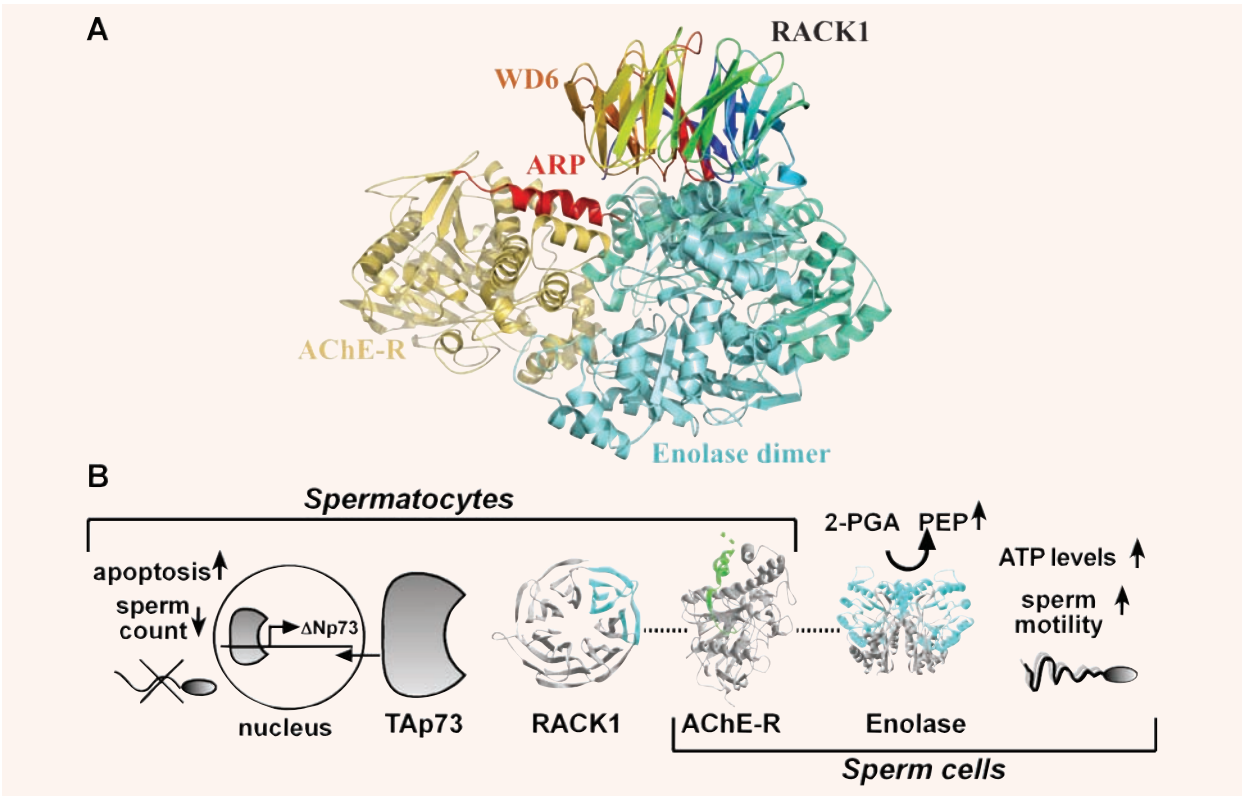

Fig. 6 AChE-R interactions with RACK1 and enolase and their consequences **A**. Possible AChE-R/RACK1/Enolase trimer. The predicted structure of a triple complex formed between the Enolase dimer (1EBH; coloured in sky blue), human AChE-R (1B41; coloured in orange) and RACK1 (modelled with Swiss Model; coloured by its sequence) were docked together using PatchDock 1.3. The C' terminus of AChE-R (ARP) is the core of the interacting triad. **B**. AChE-R interactions with RACK1 and enolase-α during spermatogenesis confer dual selection. In meiotic spermatocytes, elevated levels of AChE-R displace p73α from RACK1, resulting in elevated ΔNp73 and apoptosis of meiotic spermatocytes and reduced sperm production. In sperm, interaction with AChE-R increases enolase-α activity and glycolytic activity, which leads to elevated motility.

AChE-R function. It is interesting to speculate that AChE-R-mediated apoptosis plays parallel roles in other tissues where apoptosis is crucial for normal differentiation, for example the brain and thymus [14, 41].

AChE-R/enolase interaction elevates sperm motility by enhancing sperm metabolism

Spermatocytes and spermatids utilize lactate secreted from Sertoli cells as energy source *via* the mitochondrial tricarboxylic acid cycle (Krebs cycle) [42]. In contrast, mature, motile spermatozoa utilize glycosable substrates found in the seminal fluid to supply their high energy needs [43], and glycolysis is essential for sperm motility [21]. Therefore, glycolytic enzymes such as enolase would play more substantial roles in spermatozoa than in any other spermatogenic cell. *In vitro* incubation of enolase with the AChE-R-cleavable ARP peptide significantly elevated enolase activity. Accepted *in vitro* calculations suggest the reversible hydration reaction catalysed by enolase is in equilibrium, and hence not a rate limiting step. However, in a kinetic model of yeast glycolysis used to calculate the flux of substrates so it would fit with empirical measurements, enolase was actually far from equilibrium [44]. Moreover, in the living cell, formation of glycolytic multi-enzymatic complexes affects the flux of substrates and the efficiency of ATP production by the pathway as a whole, suggesting that multi-protein complexes can enhance

the efficiency of cellular energy metabolism [31]. Accordingly, enolase localizes to microtubules of sperm tail in an ATP-dependent manner, indicating that its juxtaposition in proximity to the mitochondrial sheath or to other glycolytic enzymes is of consequence to the metabolic status of the cell [32]. AChE, in comparison, localizes to the tail of human sperm and mouse epididymal sperm ([3] and our current data), where glycolytic enzymes are localized.

In transfected cultured cells, AChE-R elevated glucose consumption and ATP levels, suggesting augmentation of glycolysis by AChE-R/enolase-α interaction. An even greater increase in ATP levels was found in epididymal sperm from TgR mice as compared with controls, possibly because ATP levels in sperm cells depend more on glycolysis than mitochondrial activity. While mitochondrial activity alone is insufficient to produce the ATP levels required to maintain sperm motility, mitochondrial membrane potential is notably correlated with motility [23]. Therefore, mitochondrial hyperpolarization in TgR sperm predicted elevated motility compared to sperm from control mice. Indeed, CASA analysis demonstrated elevated motility and yet more intensively elevated hyperactivated motility in epdidimal sperm of TgR mice. Similarly, in human beings, separated sperm samples displayed a direct correlation between motility and AChE-R levels. Interestingly, no correlation was present in sperm samples from patients with impaired sperm properties, which also contained fewer AChE-R stained cells. This suggests that reduced AChE-R production is accompanied by formation of malfunctioning sperm with reduced motility. That enolase levels showed no association demonstrates that AChE-R's correlation with motility is not due to a gross change in protein levels in the examined sperm subpopulations. It is noteworthy that other cholinergic molecules are implicated in sperm motility. The nicotinic acetylcholine receptor is also localized to sperm tail and is required for normal sperm motility by regulating calcium influx to the cell [45]. Thus, AChE-R effects on sperm motility could involve both catalytic and non-catalytic activities.

Independent pathways weed out cells with high and low AChE-R levels

Apoptosis during the first wave of spermatogenesis is indispensable to normal adult spermatogenesis [28]. By displacing p73α from RACK1 and allowing TAp73 to activate pro-apoptotic signals in meiotic spermatocytes, AChE-R excess can reduce the number of spermatogenic cells. Interaction with enolase-α would be irrelevant at this stage, as the glycolytic pathway is not functional during germ-cell differentiation in the testis. However, in mature spermatozoa, the highly condensed chromatin is transcriptionally inactive [46], rendering it indifferent to changes in p73 levels. At this stage, AChE-R confers an advantage through its interaction with enolase-α. This increases ATP levels and motility, as seen in samples from TgR mice and fertile men. Therefore, while both AChE-R partners could be available for binding, the physiological relevance of the interaction is dependent on the characteristics of the cell type namely spermatocytes or spermatozoa. Thus, AChE-R consecutively participates in a dual selection process, excluding either AChE-R overexpressing or underexpressing sperm cells depending on the availability of ARP partners, and their function. This way, interchanging protein interactions during male germ cell differentiation can serve to evolutionarily perpetuate a moderate AChE-R level. Figure 6B presents this concept schematically. It would thus be interesting to examine in the future the consequences of RACK1 and/or enolase knockdown by siRNA.

Stress reactions are shaped by evolutionary forces, maintaining the balance between costs and benefits [47]. AChE-R serves as a stress-inducible biomarker in brain, muscle and blood [10–12]. Importantly, AChE-R overproduction confers neuroprotection from stress hallmarks [19], perhaps through AChE-R/enolase interaction and the increased cellular ATP levels. While some reports correlate reduced sperm motility following psychological stress this is not the rule [48, 49], the enhancing effect of AChE-R/enolase interaction emphasizes the complex outcome of the cellular stress response.

Taken together, our findings indicate that both the biochemical characteristics and the biological functions of AChE-R depend on its interchangeable partner proteins, and that modulation of these features affects cellular properties in a manner dependent on the differentiation stage and cellular context.

Acknowledgements

The authors are grateful to Drs. Haim Breitbart (Ramat-Gan), David Greenberg, Naomi Melamed-Book and

Sophia Diamant (Jerusalem) for support, assistance, and fruitful discussions.

This work was funded in part by DIP-3.2, EURASNET, European Alternative Splicing Network of Excellence (518238), Israel Science Foundation (618/02) and Ministry of Science (to H.S).

References

1. **Cusick ME, Klitgord N, Vidal M, Hill DE.** Interactome: gateway into systems biology. *Hum Mol Genet.* 2005; 14 Suppl 2: R17–181.
2. **Egbunike GN.** Changes in acetylcholinesterase activity of mammalian spermatozoa during maturation. *Int J Androl.* 1980; 3: 459–68.
3. **Chakraborty J, Nelson L.** Comparative study of cholinesterases distribution in the spermatozoa of some mammalian species. *Biol Reprod.* 1976; 15: 579–85.
4. **Meshorer E, Soreq H.** Virtues and woes of AChE alternative splicing in stress-related neuropathologies. *Trends Neurosci.* 2006; 29: 216–24.
5. **Birikh KR, Sklan EH, Shoham S, Soreq H.** Interaction of "readthrough" acetylcholinesterase with RACK1 and PKC{beta}II correlates with intensified fear-induced conflict behavior. *Proc Natl Acad Sci USA.* 2003; 100: 28–38.
6. **Schechtman D, Mochly-Rosen D.** Adaptor proteins in protein kinase C-mediated signal transduction. *Oncogene.* 2001; 20: 633–947.
7. **Sklan EH, Podoly E, Soreq H.** RACK1 has the nerve to act: Structure meets function in the nervous system. *Prog Neurobiol.* 2006; 78: 117–34.
8. **Perry C, Sklan EH, Soreq H.** CREB regulates AChE-R-induced proliferation of human glioblastoma cells. *Neoplasia.* 2004; 6: 279–86.
9. **Pick M, Perry C, Lapidot T, Guimaraes-Sternberg C, Naparstek E, Deutsch V, Soreq H.** Stress-induced cholinergic signaling promotes inflammation-associated thrombopoiesis. *Blood.* 2006; 107: 3397–406.
10. **Kaufer D, Friedman A, Seidman S, Soreq H.** Acute stress facilitates long-lasting changes in cholinergic gene expression. *Nature.* 1998; 393: 373–7.
11. **Brenner T, Hamra-Amitay Y, Evron T, Boneva N, Seidman S, Soreq H.** The role of readthrough acetylcholinesterase in the pathophysiology of myasthenia gravis. *Faseb J.* 2003; 17: 214–22.
12. **Grisaru D, Pick M, Perry C, Sklan EH, Almog R, Goldberg I, Naparstek E, Lessing JB, Soreq H, Deutsch V.** Hydrolytic and non-enzymatic functions of acetylcholinesterase comodulate hematopoietic stress responses. *J Immunol.* 2006; 176: 27–35.
13. **Mor I, Grisaru D, Titelbaum L, Evron T, Richler C, Wahrman J, Sternfeld M, Yogev L, Meiri N, Seidman S, Soreq H.** Modified testicular expression of stress-associated "readthrough" acetylcholinesterase predicts male infertility. *FASEB J.* 2001; 15: 2039–41.
14. **Dori A, Cohen J, Silverman WF, Pollack Y, Soreq H.** Functional manipulations of acetylcholinesterase splice variants highlight alternative splicing contributions to murine neocortical development. *Cereb Cortex.* 2005; 15: 419–30.
15. **Mochly-Rosen D, Khaner H, Lopez J.** Identification of intracellular receptor proteins for activated protein kinase C. *Proc Natl Acad Sci USA.* 1991; 88: 3997–4000.
16. **Geyer BC, Muralidharan M, Cherni I, Doran J, Fletcher SP, Evron T, Soreq H, Mor TS.** Purification of transgenic plant-derived recombinant human acetylcholinesterase-R. *Chem Biol Interact.* 2005; 157-158: 331–4.
17. **Ellman GL, Courtney D, Andres VJ, Featherstone RM.** A new and rapid colorimetric determination of acetylcholinesterase activity. *Biochem Pharmacol.* 1961; 7: 88–95.
18. **Sternfeld M, Patrick JD, Soreq H.** Position effect variegations and brain-specific silencing in transgenic mice overexpressing human acetylcholinesterase variants. *J Physiol.* 1998; 92: 249–55.
19. **Sternfeld M, Shoham S, Klein O, Flores-Flores C, Evron T, Idelson GH, Kitsberg D, Patrick JW, Soreq H.** Excess "readthrough" acetylcholinesterase attenuates but the "synaptic" variant intensifies neurodeterioration correlates. *Proc Natl Acad Sci USA.* 2000; 97: 8647–52.
20. **Seidman S, Sternfeld M, Ben Aziz-Aloya R, Timberg R, Kaufer-Nachum D, Soreq H.** Synaptic and epidermal accumulations of human acetylcholinesterase are encoded by alternative 3'-terminal exons. *Mol Cell Biol.* 1995; 15: 2993–3002.
21. **Miki K, Qu W, Goulding EH, Willis WD, Bunch DO, Strader LF, Perreault SD, Eddy EM, O'Brien DA.** Glyceraldehyde 3-phosphate dehydrogenase-S, a sperm-specific glycolytic enzyme, is required for sperm motility and male fertility. *Proc Natl Acad Sci USA.* 2004; 101: 16501–6.
22. **Gur Y, Breitbart H.** Mammalian sperm translate nuclear-encoded proteins by mitochondrial-type ribosomes. *Genes Dev.* 2006; 20: 411–6.
23. **Garner DL, Thomas CA, Joerg HW, DeJarnette JM, Marshall CE.** Fluorometric assessments of mitochondrial function and viability in cryopreserved bovine spermatozoa. *Biol Reprod.* 1997; 57: 1401–6.
24. **Malkov M, Fisher Y, Don J.** Developmental schedule of the postnatal rat testis determined by flow cytometry. *Biol Reprod.* 1998; 59: 84–92.
25. **Alvarez A, Alarcon R, Opazo C, Campos EO, Munoz FJ, Calderon FH, Dajas F, Gentry MK, Doctor BP, De Mello FG, Inestrosa NC.** Stable complexes involving acetylcholinesterase and amyloid-beta

peptide change the biochemical properties of the enzyme and increase the neurotoxicity of Alzheimer's fibrils. *J Neurosci.* 1998; 18: 3213–23.

26. **Lax Y, Rubinstein S, Breitbart H.** Subcellular distribution of protein kinase C alpha and betaI in bovine spermatozoa, and their regulation by calcium and phorbol esters. *Biol Reprod.* 1997; 56: 454–9.
27. **Shima JE, McLean DJ, McCarrey JR, Griswold MD.** The murine testicular transcriptome: characterizing gene expression in the testis during the progression of spermatogenesis. *Biol Reprod.* 2004; 71: 319–30.
28. **Rodriguez I, Ody C, Araki K, Garcia I, Vassalli P.** An early and massive wave of germinal cell apoptosis is required for the development of functional spermatogenesis. *Embo J.* 1997; 16: 2262–70.
29. **Hamer G, Gademan IS, Kal HB, de Rooij DG.** Role for c-Abl and p73 in the radiation response of male germ cells. *Oncogene.* 2001; 20: 4298–304.
30. **Ozaki T, Watanabe K, Nakagawa T, Miyazaki K, Takahashi M, Nakagawara A.** Function of p73, not of p53, is inhibited by the physical interaction with RACK1 and its inhibitory effect is counteracted by pRB. *Oncogene.* 2003; 22: 3231–42.
31. **Merkulova T, Lucas M, Jabet C, Lamande N, Rouzeau JD, Gros F, Lazar M, Keller A.** Biochemical characterization of the mouse muscle-specific enolase: developmental changes in electrophoretic variants and selective binding to other proteins. *Biochem J.* 1997; 323: 791–800.
32. **Gitlits VM, Toh BH, Loveland KL, Sentry JW.** The glycolytic enzyme enolase is present in sperm tail and displays nucleotide-dependent association with microtubules. *Eur J Cell Biol.* 2000; 79: 104–11.
33. **Mizukami Y, Iwamatsu A, Aki T, Kimura M, Nakamura K, Nao T, Okusa T, Matsuzaki M, Yoshida K, Kobayashi S.** ERK1/2 regulates intracellular ATP levels through alpha-enolase expression in cardiomyocytes exposed to ischemic hypoxia and reoxygenation. *J Biol Chem.* 2004; 279: 50120–31.
34. **Ho HC, Granish KA, Suarez SS.** Hyperactivated motility of bull sperm is triggered at the axoneme by Ca2+ and not cAMP. *Dev Biol.* 2002; 250: 208–17.
35. **Gaur U, Aggarwal BB.** Regulation of proliferation, survival and apoptosis by members of the TNF superfamily. *Biochem Pharmacol.* 2003; 66: 1403–8.
36. **Shivakrupa R, Radha V, Sudhakar C, Swarup G.** Physical and functional interaction between Hck tyrosine kinase and guanine nucleotide exchange factor C3G results in apoptosis, which is independent of C3G catalytic domain. *J Biol Chem.* 2003; 278: 52188–94.
37. **Podar K, Mostoslavsky G, Sattler M, Tai YT, Hayashi T, Catley LP, Hideshima T, Mulligan RC, Chauhan D, Anderson KC.** Critical role for hematopoietic cell kinase (Hck)-mediated phosphorylation of Gab1 and Gab2 docking proteins in interleukin 6-induced proliferation and survival of multiple myeloma cells. *J Biol Chem.* 2004; 279: 21658–65.
38. **Lopez-Bergami P, Habelhah H, Bhoumik A, Zhang W, Wang LH, Ronai Z.** Receptor for RACK1 mediates activation of JNK by protein kinase C. *Mol Cell.* 2005; 19: 309–20.
39. **Yang A, Kaghad M, Caput D, McKeon F.** On the shoulders of giants: p63, p73 and the rise of p53. *Trends Genet.* 2002; 18: 90–5.
40. **Nakagawa T, Takahashi M, Ozaki T, Watanabe K, Hayashi S, Hosoda M, Todo S, Nakagawara A.** Negative autoregulation of p73 and p53 by DeltaNp73 in regulating differentiation and survival of human neuroblastoma cells. *Cancer Lett.* 2003; 197: 105–9.
41. **Hogquist KA, Baldwin TA, Jameson SC.** Central tolerance: learning self-control in the thymus. *Nat Rev Immunol.* 2005; 5: 772–82.
42. **Grootegoed JA, Jansen R, Van der Molen HJ.** The role of glucose, pyruvate and lactate in ATP production by rat spermatocytes and spermatids. *Biochim Biophys Acta.* 1984; 767: 248–56.
43. **Storey BT, Kayne FJ. Energy metabolism of spermatozoa. V.** The Embden-Myerhof pathway of glycolysis: activities of pathway enzymes in hypotonically treated rabbit epididymal spermatozoa. *Fertil Steril.* 1975; 26: 1257–65.
44. **Teusink B, Passarge J, Reijenga CA, Esgalhado E, van der Weijden CC, Schepper M, Walsh MC, Bakker BM, van Dam K, Westerhoff HV, Snoep JL.** Can yeast glycolysis be understood in terms of *in vitro* kinetics of the constituent enzymes? Testing biochemistry. *Eur J Biochem.* 2000; 267: 5313–29.
45. **Bray C, Son JH, Kumar P, Meizel S.** Mice deficient in CHRNA7, a subunit of the nicotinic acetylcholine receptor, produce sperm with impaired motility. *Biol Reprod.* 2005; 73: 807–14.
46. **Grunewald S, Paasch U, Glander HJ, Anderegg U.** Mature human spermatozoa do not transcribe novel RNA. *Andrologia.* 2005; 37: 69–71.
47. **Korte SM, Koolhaas JM, Wingfield JC, McEwen BS.** The Darwinian concept of stress: benefits of allostasis and costs of allostatic load and the trade-offs in health and disease. *Neurosci Biobehav Rev.* 2005; 29: 33–8.
48. **Zorn B, Auger J, Velikonja V, Kolbezen M, Meden-Vrtovec H.** Psychological factors in male partners of infertile couples: relationship with semen quality and early miscarriage. *Int J Androl.* 2007, in press; DOI: 10.1111/j.1965-2605.2007.00806.x
49. **Zorn B, Sucur V, Stare J, Meden-Vrtovec H.** Decline in sex ratio at birth after 10-day war in Slovenia: brief communication. *Hum Reprod.* 2002; 17: 3173–7.
50. **Bonet J, Caltabiano G, Khan AK, Johnston MA, Corbi C, Gomez A, Rovira X, Teyra J, Villa-Freixa J.** The role of residue stability in transient protein-protein interactions involved in enzymatic phosphate hydrolysis. A computational study. *Proteins.* 2006; 63: 65–77.